Science of Sintering, **51** (2019) 363-376

doi:https://doi.org/10.2298/SOS1904363O

UDK: 666.3.019; 532.74; 622.785

Characterization of $MgAl_2O_4$ Sintered Ceramics

Nina Obradović[1*)], William G. Fahrenholtz[2], Suzana Filipović[1], Cole Corlett[2], Pavle Đorđević[1], Jelena Rogan[3], Predrag J. Vulić[4], Vladimir Buljak[5], Vladimir Pavlović[1]

[1]Institute of Technical Sciences of the Serbian Academy of Sciences and Arts, 11000 Belgrade, Serbia

[2]Materials Science and Engineering, Missouri University of Science and Technology, Rolla, Missouri, United States

[3]Department of General and Inorganic Chemistry, Faculty of Technology and Metallurgy, University of Belgrade, 11120 Belgrade, Serbia

[4]Faculty of Mining and Geology, University of Belgrade, 11000 Belgrade, Serbia

[5]Faculty of Mechanical Engineering, University of Belgrade, 11000 Belgrade, Serbia

Abstract:

Single phase $MgAl_2O_4$ was made from a one-to-one molar ratio of MgO and Al_2O_3 powders mixed using ball-milling. Mixtures of MgO and Al_2O_3 were subsequently treated in planetary ball mill for 30, 60, 90 and 120 minutes in air. The aim of this study was to examine phase composition, microstructure, and densification behavior of sintered specimens. After sintering in dilatometer at 1500 °C, the powder was converted to single phase $MgAl_2O_4$. The results show that mechanical activation improved the densification behavior of $MgAl_2O_4$ sintered specimens, and it reduced the onset temperature for sintering by approx. 100 °C. Based on dilatometer data, powders were subsequently densified at 1450 °C by hot pressing. Almost all specimens exhibited full density, while sample activated for 30 minutes showed the fastest densification rate.

***Keywords**: Mechanical activation; Sintering; XRD; SEM; Spinel.*

1. Introduction

Magnesium aluminate, $MgAl_2O_4$, the only compound in the MgO-Al_2O_3 binary system, is a refractory ceramic of great importance in modern technologies [1]. It possesses attractive physico-chemical properties, such as high melting point (> 2100 °C), high hardness and resistance to chemical attack, making it useful in high-temperature applications [2]. Due to low dielectric constant (~ 8), it can also be used as a dielectric in microwave applications [3]. When fully dense, pure $MgAl_2O_4$ can be transparent [4]. Owing to high mechanical strength and low cost, spinel ceramics have been used as transparent armor, infrared windows, domes for missiles and laser host materials [1, 5]. $MgAl_2O_4$ compound can be synthesized through various techniques, such as direct solid-state reaction, ultrasonic treatment, gel casting, wet chemical solution techniques, co-precipitation, and mechano-chemical reaction [6-15].

*) **Corresponding author:** nina.obradovic@itn.sanu.ac.rs (Dr. Nina Obradović)

Recently, with the continuous innovation of sintering technology, increasing numbers of different sintering techniques have been used to prepare $MgAl_2O_4$ ceramics, including: spark plasma sintering [16], pressure assisted microwave sintering [17], pressureless sintering [13], reactive sintering followed by HIP [5], dilatometry [18], and the most advanced hot pressing (HP) [19]. In particular, HP has been recognized as an advanced method for ceramic fabrication. HP is a fast and effcient sintering technique that uses high pressure low-strain-rate powder metallurgy process for forming of a powder or powder compact at a temperature high enough to induce sintering and creep processes [20]. Typically, HP can use high heating rates (50 °C/min or higher) and short non-isothermal sintering times (30 min or less) and it is considered an excellent method for preparing nanostructured ceramics and nanocomposites [20, 21]. Compared to conventional sintering processes, HP can significantly shorten the sintering time (i.e., just a few minutes) and promote full densification of materials that are diffcult to sinter using conventional sintering techniques. The key issue in all sintering approaches is controlling the grain growth/densification behavior. During conventional sintering of ceramics, grain growth usually occurs during the final stage of processing when relative density is ~ 90 % or higher. When grain growth starts, it affects the densification kinetics because the grain size has a direct influence on the length of the diffusional path and the surface forces that govern sintering. In consequence, grain growth decreases the densification rate of powder compacts during the final sintering stage of sintering [22].

The goal of this study is to demonstrate the possibility of achieving fully dense pure $MgAl_2O_4$ spinel ceramics from as-received commercial powders by a process that combined mechanical activation and hot pressing. The sintering process was simulated by employing numerical Finite Element Model (FEM) and the influence of mechanical activation on final microstructures, grain growth and final densities was examined.

2. Materials and Experimental Procedures

A mixture of high-purity MgO (99.9 % purity Sigma–Aldrich, p.a.) and α-Al_2O_3 (A16-SG, Almatis) starting powders were used in these experiments. The starting MgO and α-Al_2O_3 powders were added in a one-to-one molar ratio and mixed by ball milling. The powder mixture was mechanically activated for 30, 60, 90 or 120 minutes in a high-energy planetary ball mill (Planetary Ball Mill Retsch PM 100) in air. Mechanical activation was performed by using Y-stabilized ZrO_2 vials and balls. The milling balls were 5 mm in diameter. The ball-to-powder weight ratio was 30:1 with a rotation speed of 400 rpm. Powders were sieved after milling. The powder mixtures were labeled based on the activation time as AM–0 up to AM–120.

Average particle size and particle size distribution were determined by a laser light-scattering particle size analyzer (PSA; Mastersizer 2000, Malvern Instruments Ltd., UK), covering the particle size range of 0.02–2000 μm. For the PSA measurements, the powders were dispersed in distilled water in an ultrasonic bath (low-intensity ultrasound, at a frequency of 40 kHz and power of 50 W) for 5 minutes. Specific surface area was measured using nitrogen adsorption with analysis by the BET method (Autosorb, Quantachrome, Boynton Beach, FL). The morphology of the powders and sintered specimens was analyzed by the scanning electron microscopy (SEM; JEOL JSM-6390 LV). Prior to SEM observations, the powders and crushed sintered samples were coated with gold to minimize charging. Every micrograph is processed by ImageJ program package, and distributions are determined by measuring at least 50 grains [23]. The phase composition of powders was identified based on X-ray diffraction (XRD) patterns obtained on a Philips PW-1050 diffractometer with Cu-K_α radiation (λ=1.5418 Å) and a step/time scan mode of 0.05 $^{o}\cdot s^{-1}$ in the 2θ range 15–90 ^{o}.

The binder-free powders were compacted at 300 MPa using a uniaxial double action pressing process with an 8 mm diameter tool (hydraulic press RING, P-14, VEB THURINGER). Compacts were placed in a dilatometer (SETSYS Evolution TMA, Setaram Instrumentation, Caluire, France). Dilatometric curves were obtained after sintering in air, at temperatures ranging from 25 °C to 1500 °C, with heating rates of 10 °C·min^{-1}. The bulk densities were calculated from measurements of mass, diameter, and thickness of the sintered specimens. After sintering, the sintering temperatures were added to the specimen designations such that AM–120–1500 indicates a specimen that was produced from powder that was mechanically activated for 120 minutes and sintered at 1500 °C. The theoretical density (TD) of $MgAl_2O_4$ was assumed to be 3.58 g·cm^{-3} based on previous reports [24]. The mechanical behavior of sintered material is modeled through phenomenological visco-elasto-plastic constitutive model designed to study the densification during the sintering process. Powder compacts were discontinuous due to the presence of internal voids (i.e., porosity) within the material. The adopted modeling strategy focused only on global, phenomenological aspects of thermo-mechanical response, so the material was treated as a continuum, with relative density related to equivalent inelastic deformation. A similar approach has been adopted in previous works related to numerical modeling of powder compaction and sintering [25, 26]. The employed constitutive model is implemented in a UMAT subroutine within a commercial code (ABAQUS) [27].

XRD patterns for pulverized sintered specimens were collected using a Rigaku SmartLab automated powder X-ray diffractometer with Cu-$K_{\alpha 1,2}$ (λ=1.5406 Å) radiation (U = 40 kV, I = 30 mA) equipped with D/teX Ultra 250 stripped 1D detector in the XRF reduction mode. The diffraction angle range was 10–120 °.

Hot pressing (HP-3060-20, Thermal Technology, Santa Rosa, CA) was conducted using a heating rate of 10 °C/min to the desired isothermal temperature where it was held for 30 min. A uniaxial load of 32 MPa was applied when the temperature was above 1200 °C. Densification behavior was recorded using a linearly variable differential transducer attached to the hot-press rams. Time-dependent density values were calculated using Eq. (1):

$$\rho_t = \frac{\rho_f}{\left(1+\frac{L_t}{L_f}\right)} \qquad (1)$$

where L_f is final length, L_t is the change in length at time t, ρ_t is the relative density at time t, and ρ_f is the final relative density. The furnace was cooled at ~ 20 °C/min and the load was released at 1200°C. After HP, the sintering temperatures were added to the specimen designations such that AM–120–1450 indicates a specimen that was produced from powder that was mechanically activated for 120 minutes and hot pressed at 1450 °C. Densities were measured based on Archimedes principle using water as the immersion medium.

3. Results and Discussion

The results of the particle size analysis of the non-activated and mechanically activated powders are presented in Fig. 1. The average particle size d(0.5) was 1.8 μm for the non-activated powder AM–0.

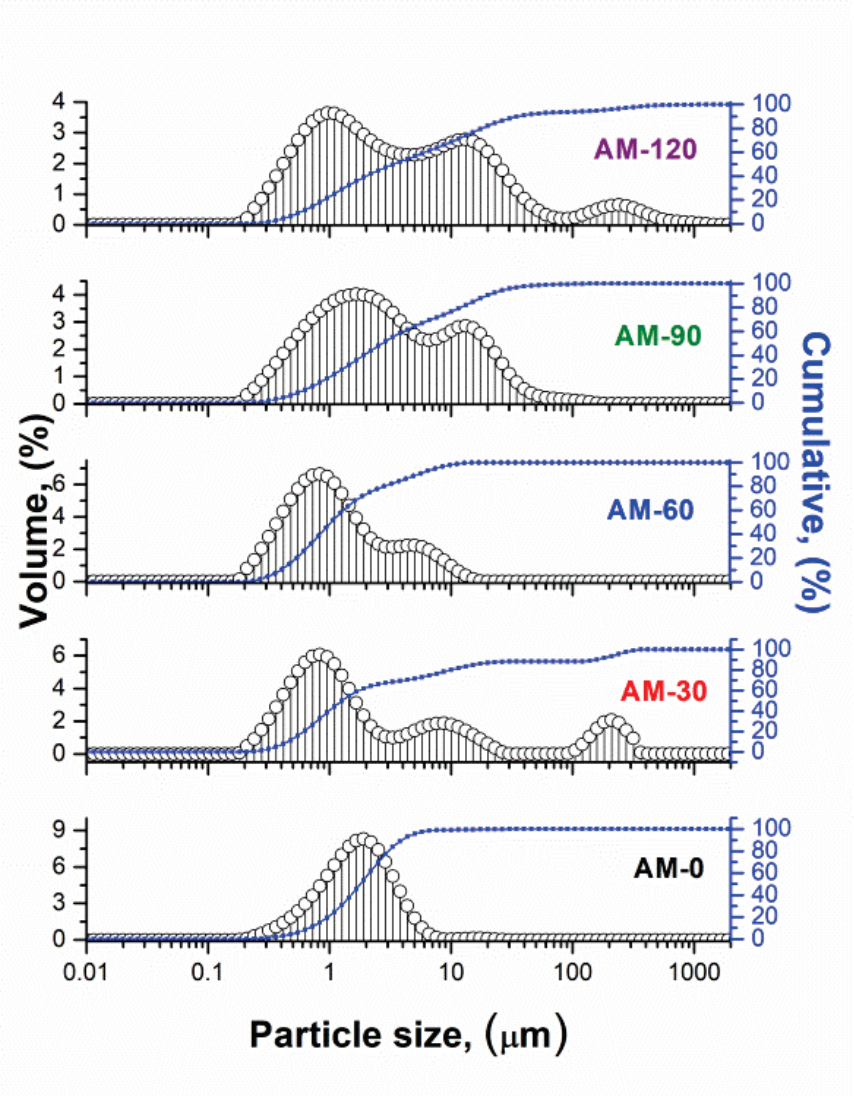

Fig. 1. Particle size analysis of non-activated and mechanically activated powders.

After mechanical activation for 30 minutes, the average particle size decreased to about 1.3 μm, reaching the minimum of 1.1 μm for the powder activated for 60 minutes. With the prolonged milling time, d(0.5) increased to 2.7 and 3.4 μm for AM–90 and AM–120, respectively. Likewise, d(0.1) decreased from 0.7 μm for AM–0 to 0.4 μm for AM–60, and increased again to 0.6 μm for AM–120. Interestingly, d(0.9) increased from 3.9 μm for AM–0 to 157.8 μm for AM–30, then decreased to 5.5 for AM–60. Further activation led to the increase in d(0.9) value up to 19.8 and 35.6 μm for AM–90 and AM–120, respectively. Milling also produced a bi-modal or tri-modal particle size distribution in the activated powders, indicating agglomeration. Milling reduced the average particle size [28]; it also produced agglomerates (soft agglomerates for lower milling times and hard agglomerates for powders activated more than 60 minutes) that were larger than in the starting powder, and indicated that powder activated for 60 minutes had the lowest average particle size along with crushed soft agglomerates.

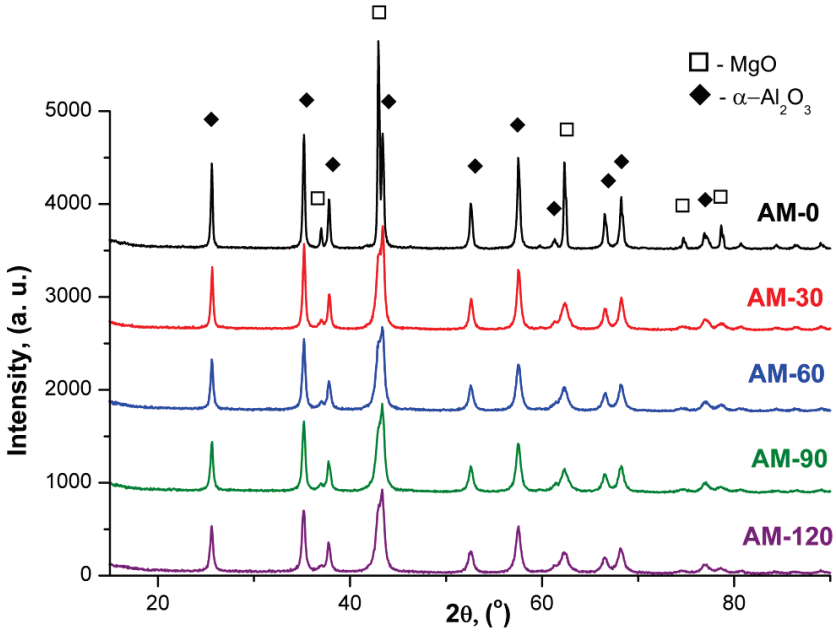

Fig. 2. XRD patterns of non-activated and mechanically activated powders.

The phase composition of the non-activated and activated powders is presented in Fig. 2. All diffraction lines were identified using corresponding JCPDS cards: 74–1081 for α-Al_2O_3 and 45–0946 for MgO. A mixture of the starting oxides (α-Al_2O_3 and MgO) was detected in the non-activated powder (AM–0). The sharp, intense peaks indicated the microcrystalline nature of the starting components. The same phases were detected within all activated powders. No new phases were obtained during milling. However, the intensities of the peaks decreased and the peaks were broadened, which is characteristic of reduction of crystallite size and increased strain in the mechanically activated powders [29].

Tab. I represents results of specific surface area along with microstructural parameters of non-activated and activated powders. Values of specific surface area are consistent with PSA results; SSA exhibits the maximum at 9.8 $m^2 \cdot g^{-1}$ for the powder activated 60 minutes indicating the smallest particle size. Values of crystallite size and microstrain were calculated based on XRD results. The decrease in crystallite size along with increase in microstrain is characteristic of activated powders. Hence, mechanical activation increases disorder of the crystal structure and introduces defects into the powder particles [30].

Tab. I Specific surface area and microstructural parameters of non-activated and mechanically activated powders.

Sample	SSA ($m^2 \cdot g^{-1}$)	Crystallite size (nm)		Microstrain (%)	
		MgO	Al_2O_3	MgO	Al_2O_3
MA–0	6.3	91	107	0.00	0.10
MA–30	7.4	87	98	0.45	0.23
MA–60	9.8	41	36	0.38	0.21
MA–90	7.8	36	57	0.39	0.22
MA–120	9.1	31	70	0.41	0.28

Scanning electron micrographs are presented in Fig. 3. Non-activated powder consisted of two different types of powder particles. The first type was smaller, around 500 nm in diameter. The second type of particles was larger, with polygonal shapes. These particles ranged in size from about 1.5 μm to 2.5 μm across. The attrition of powder particles is evident for all activated powders. The powder activated 60 minutes appeared to be homogeneous with the smallest particles around 400 nm in diameter. Clustering of particles and formation of agglomerates were observed in AM–90 and AM–120 powders, which is a common phenomenon for powders that have been subjected to prolonged activation [31].

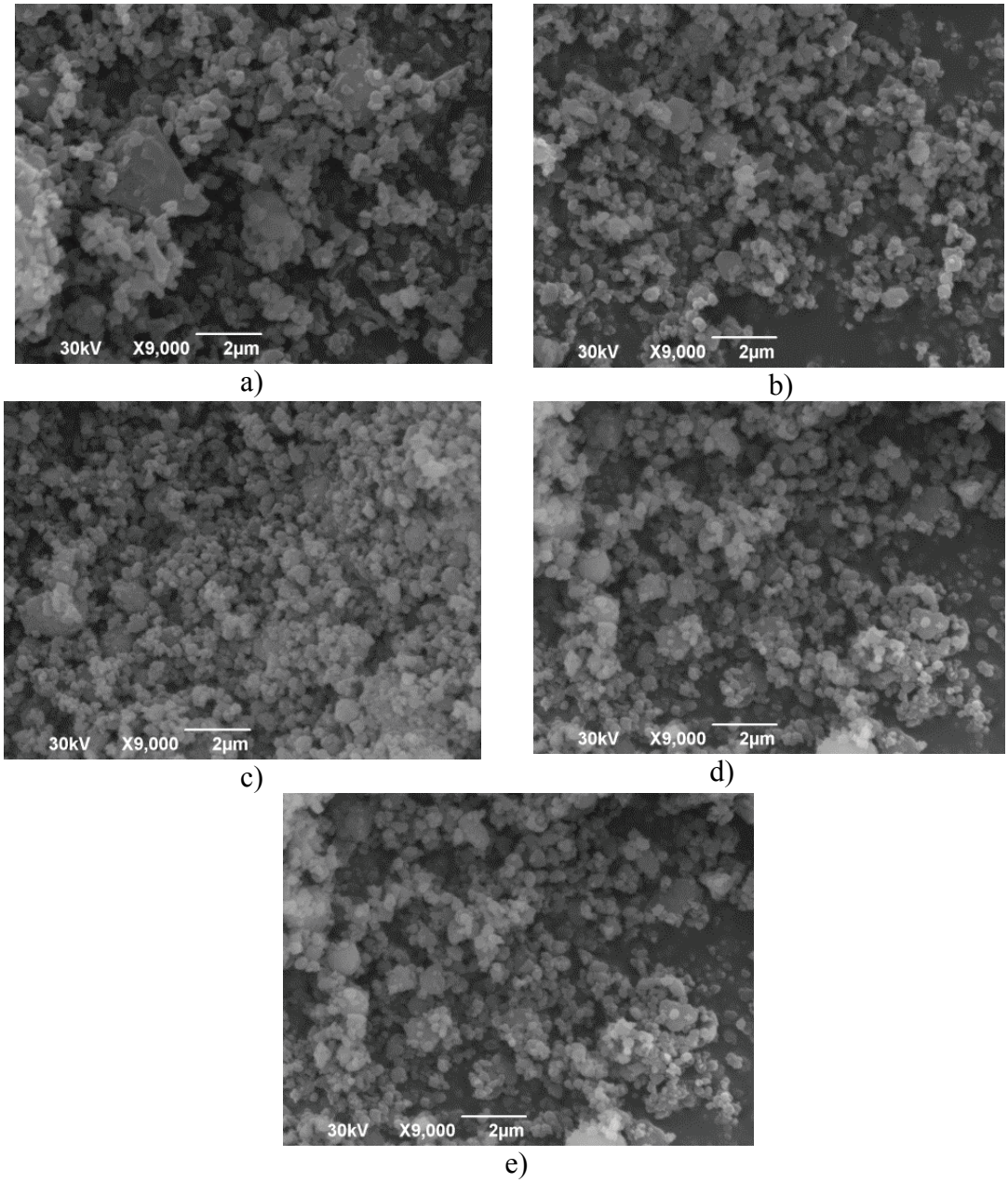

Fig. 3. SEM micrographs of powders: a) AM–0, b) AM–30, c) AM–60, d) AM–90, and e) AM–120.

All powders were compacted prior to dilatometry. Densities of compacted powders before sintering were between 61 and 63 % TD. Dilatometric curves of non-activated and activated powders are presented in Fig. 4. The expansion due to spinel formation and shrinkage due to sintering occur sequentially with the increase in temperature [18]. The dilatometric plot clearly shows that mechanical activation reduces the onset temperature for the spinel formation reaction, which leads to expansion at lower temperatures. After sintering at 1500 °C, the lowest density was obtained for non-activated powder, which only reached around 61 % TD. All activated sintered specimens possess densities in the range 75-79 % TD (see Tab. II). The volume expansion (approx. 8 %) associated with spinel phase formation from alumina and magnesia inhibits formation of dense bodies in a single-stage reaction sintering process [24]. Also, as the time of mechanical activation increased, the temperature corresponding to the onset of shrinkage noticeably decreased from ~ 1409 °C in AM–0 to ~ 1340 °C in AM–120 [32, 33]. Furthermore, with the prolonged mechanical activation, the apparent decrease in expansion was due to the lower energy needed for spinel reaction [18]. Moreover, shrinkage was more uniform in all directions for activated specimens as both the height and diameter were lowered after sintering, but only the decrease in height was captured by the dilatometer. Powders were more reactive after activation, so less energy and lower temperatures were required for sintering [34].

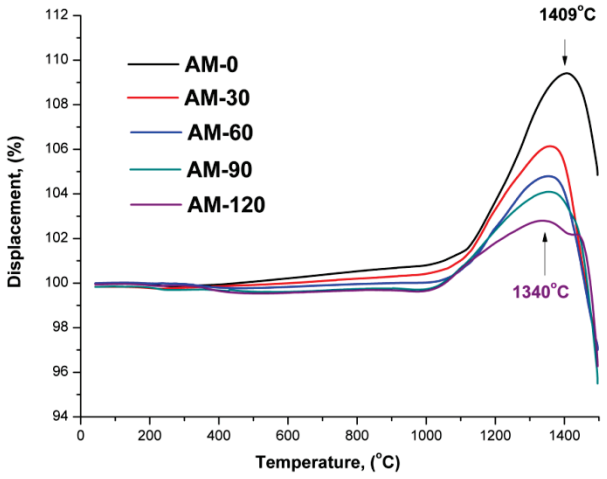

Fig. 4. Dilatometric curves of powders sintered up to 1500 °C.

Tab. II Densities of pellets sintered in dilatometer.

Sample	ρ (g·cm^{-3})	% TD
AM–0–1500	2.20	61.5
AM–30–1500	2.72	76.0
AM–60–1500	2.70	75.6
AM–90–1500	2.74	76.5
AM–120–1500	2.81	78.6

Numerical analysis of sintering offered insight into the porosity distribution over the pellets, which can be rather important for specimens of complex shape. Geometrically, specimens are axially symmetric, however in a view of exploiting the local heterogeneity of relative density distribution; they are modeled as 3D bodies, with C3D8T, coupled thermo-mechanical finite elements. To reduce computing time, symmetry was exploited, therefore only one quarter of the specimen was modeled, with symmetric boundary conditions prescribed on each cut surface. Fig. 5 visualizes the adopted finite element mesh with initial

distribution of relative density (RD). In this study, random normal distribution over the specimen, with ± 15 % (see legend on the Fig. 5) with respect to the experimentally measured mean value of RD of the sample was adopted. Alternatively, real measurement of distribution of RD (not available here), or numerical results achieved through powder compaction simulation can used as input to the sintering simulation [25].

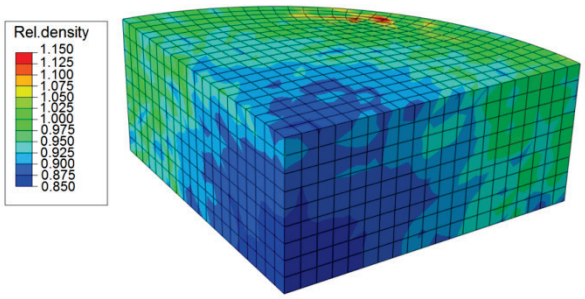

Fig. 5. One-quarter of sample and the adopter FE mesh for sintering simulation, with distribution of RD over the specimen.

The XRD patterns of heat treated powders are presented in Fig. 6. All reflections were identified using the corresponding JCPDS card 33–0853 for $MgAl_2O_4$. All peaks were sharp, indicating that the MgO and Al_2O_3 powders reacted to form the crystalline $MgAl_2O_4$ spinel. No peaks belonging to MgO and Al_2O_3 were apparent when the entire pattern was observed. Also, no peaks were observed for ZrO_2, which could have been introduced as contamination into the powder during mechanical activation that used zirconia vial and milling balls. According to literature data, the temperature range of 950–1400 °C corresponds to spinel formation [35]. Heating to temperatures of 1500 °C resulted in the formation of pure spinel, even for the non-activated powder.

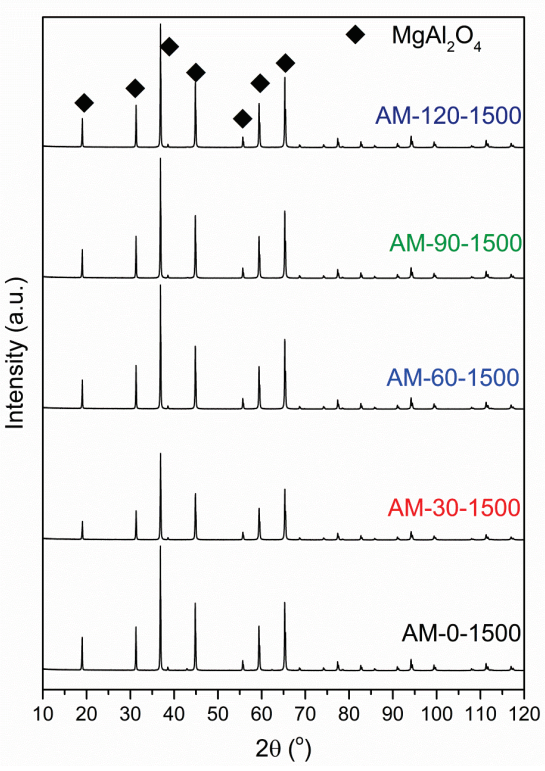

Fig. 6. XRD patterns of specimens sintered at 1500 °C.

Scanning electron micrographs of fracture surfaces of the specimens sintered in the dilatometer along with grain size distributions are presented in Fig. 7. The non-activated sintered specimen consisted of grains around 500 nm with necks that formed during sintering (first and second sintering stage), with a great amount of open porosity. Activated and sintered specimens had two regions; the first one is like the microstructure of AM–0–1500, representing the initial sintering stage.

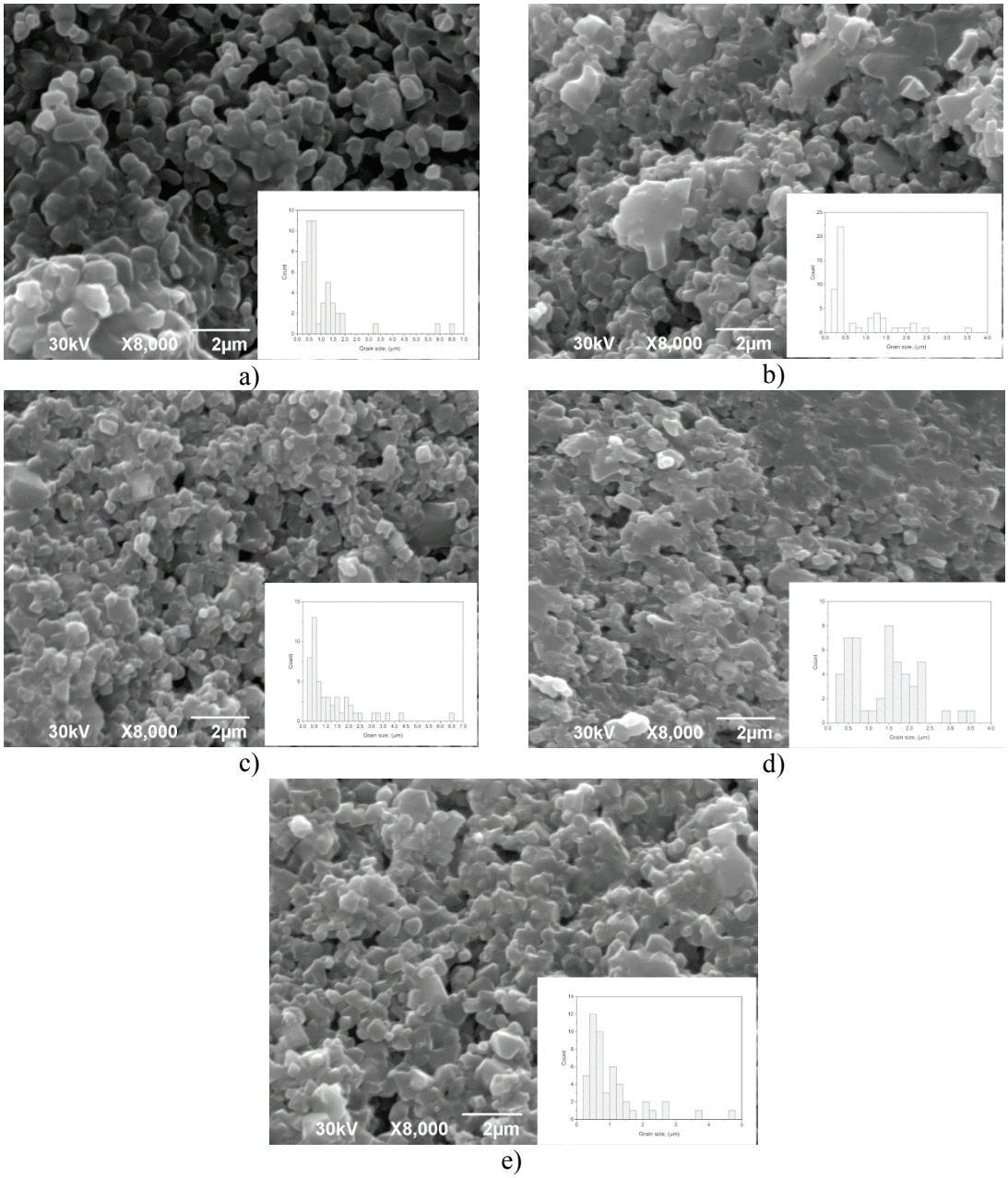

Fig. 7. SEM micrographs of fracture surfaces of sintered specimens: a) AM–0–1500, b) AM–30–1500, c) AM–60–1500, d) AM–90–1500, and e) AM–120–1500.

The other one represents blocks of well sintered regions, with grains approx. 2 μm in diameter, and small closed pores, indicating that second sintering stage had been reached (closed pores, grain growth, and densification). The relatively slow densification in the

dilatometer and temperature limit of 1500 °C were not sufficient for obtaining full density; samples did not reach the third sintering stage. The most homogeneous microstructure was noticed within specimens activated for 30 and 60 minutes, probably as the consequence of initial microstructure, high specific surface area along with microstructural parameters. Analysis of grain distribution is in accordance with microstructures, indicating that most of the grains were below 0.5 μm in diameter.

Tab. III shows the values of density for the HP specimens. The non-activated specimen had a density near 99 %, while all activated specimens exhibited full density, indicating temperature of 1450 °C along with a pressure of 32 MPa and a few minutes of sintering time were sufficient for final sintering stage and full densification. Specimen AM–30–1450 had the highest densification rate 0.17 $g \cdot cm^{-3} \cdot min^{-1}$, compared to other sintered specimens that had densification rates in the range of 0.10-0.11 $g \cdot cm^{-3} \cdot min^{-1}$.

Tab. III Densities of pellets sintered in hot press.

Sample	ρ ($g \cdot cm^{-3}$)	% TD
AM–0–1450	3.53	98.7
AM–30–1450	3.58	100.0
AM–60–1450	3.58	99.9
AM–90–1450	3.57	99.8
AM–120–1450	3.59	100.0

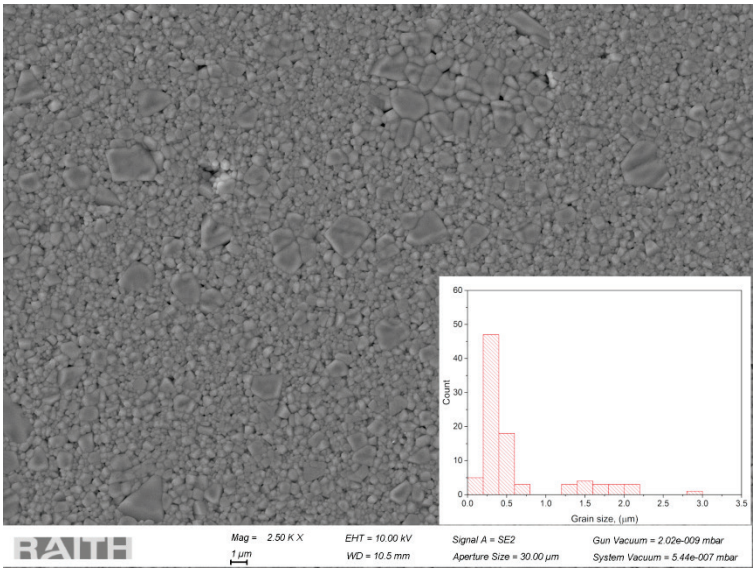

Fig. 8. SEM micrograph of AM–0–1450 hot-pressed specimen.

Scanning electron micrograph of the non-activated and hot pressed specimen (AM–0–1450) is presented in Fig. 8. Unlike SEM obtained after dilatometry, after hot pressing the grain size distribution was more even with an average grain size around 0.3 μm. The non-activated specimen had a small fraction of porosity that appeared to be in the range of 200-500 nm in diameter. The other specimens contained a mixture of small (200-500 nm diameter) and large (> 1 μm in diameter) grains that require further analysis.

The numerical model was used to simulate sintering in the dilatometer. Governing parameters entering into the adopted constitutive model were assessed following the inverse

analysis procedure, centered on minimization of the difference between experimentally measured dilatometric curves, and their computed counterparts [36]. Since the simulation was thermo-mechanical, several constitutive parameters were treated as temperature dependent. The adopted numerical model provided an accurate qualitative representation of the complete sintering process. Five samples represented in Fig. 4 were used as inputs to the procedure, all resulting in excellent agreement with experimental curves. Typical example is visualized in the Fig. 9 for the sample AM–30, the other omitted for brevity. The hot press method employed in this study is not subjected to numerical modeling since it achieved 100 % theoretical density at the end of the sintering process.

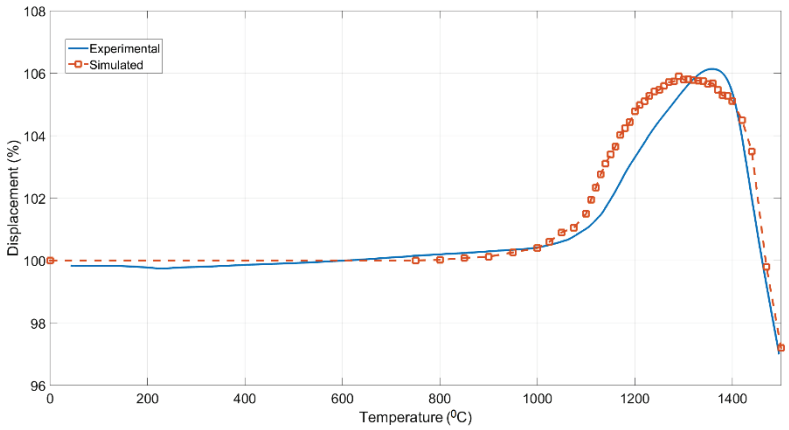

Fig. 9. Comparison of simulated and experimental dilatometric curves for the sample AM–30.

4. Conclusion

The influence of mechanical activation on sintering of spinel ceramics was investigated. $MgAl_2O_4$ ceramics were prepared by solid state reaction between MgO and α-Al_2O_3 powders during conventional sintering in a dilatometer and by hot pressing. Prior to heating, part of powder mixture was subjected to high energy planetary ball milling. The phase composition, microstructure, and densities of the bulk materials were characterized systematically.

The high-energy ball milling led to reduction of particle size and introduction of defects. Pure $MgAl_2O_4$ spinel was formed by sintering in dilatometer at 1500 °C. Mechanical activation affected the onset of sintering temperature, lowering it by ~100 °C. Densities and microstructures showed that specimens after dilatometry reached almost 78 % TD, with a great amount of open porosity, which indicated that the specimens had entered the second sintering stage. Non-activated specimens reached 98.6 % TD after hot pressing, while activated specimens reached full densities, with no porosity, which indicated that these materials entered the third final sintering stage.

The numerical model provided a qualitative description of the sintering process. Reliability of the model can be verified by comparing the overall thermo-mechanical response of the specimen during sintering, described by dilatometric curves. Simulated results contain also local distribution of the porosity over the sample, through inelastic deformation of modeled continuum. This quantity was not presented in this work as there was no experimental data available for the comparison, but potentially can provide important information regarding the sintering process.

Acknowledgments

This investigation was supported by the Serbian Ministry of Education, Science and Technological Development of the Republic of Serbia, and it was conducted under the following projects: OI 172057, and III 45007. The authors would like to thank Dr. Miodrag Mitrić and Dr. Smilja Marković for XRD, PSA and dilatometer measurements.

5. References

1. M. Sadegh Abdi, T. Ebadzadeh, A. Ghaffari, et al., Synthesis of nano-sized spinel ($MgAl_2O_4$) from short mechanochemically activated chloride precursor and its sintering behavior, Adv. Powd. Technol. 26 (2015) 175-179.
2. Z. Quan, Z. Wang, X. Wang, et al., Effect of CeO_2 addition on the sintering behavior of pre-synthesized magnesium aluminate spinel ceramic powders, Ceram. Inter. 45 (2019) 488-493.
3. A. Zegadi, M. Kolli, M. Hamidouche, et al., Transparent $MgAl_2O_4$ spinel fabricated by spark plasma sintering from commercial powders, Ceram. Int. 44 (2018) 18828-18835.
4. M. R. du Merac, H.-J. Kleebe, M. M. Müller, I. E. Reimanis, Fifty Years of Research and Development Coming to Fruition; Unraveling the Complex Interactions during Processing of Transparent Magnesium Aluminate ($MgAl_2O_4$) Spinel, J. Am. Ceram. Soc. 96(11) (2013) 3341-3365.
5. D. Han, J. Zhang, P. Liu, et al., Densification and microstructure evolution of reactively sintered transparent spinel ceramics, Ceram. Int. 44 (2018) 11101-11108.
6. M. M. Khorramirad, M. R. Rahimipour, S. M. M. Hadavi, et al., The effect of magnesium compounds (MgO and $MgAl_2O_4$) on the synthesis of Lanthanum magnesium hexaaluminate ($LaMgAl_{11}O_{19}$) by solid-state reaction method, Ceram. Inter. 44 (2018) 4734-4739.
7. -N. Rahmat, Z. Yaakob, M. Pudukudy, et al., Single step solid-state fusion for $MgAl_2O_4$ spinel synthesis and its influence on the structural and textural properties, Powd. Technol. 329 (2018) 409-419.
8. R. Raghu, J. Nampoothiri, T. Satish Kumar, In-situ generation of $MgAl_2O_4$ particles in Al-Mg alloy using H_3BO_3 addition for grain refinement under ultrasonic treatment, Measur. 129 (2018) 389-394.
9. H. Shahbazi, M. Tataei, A novel technique of gel-casting for producing dense ceramics of spinel ($MgAl_2O_4$), Ceram. Inter. 45 (2019) 8727-8733.
10. J. Bai, J. Liu, C. Li, et al., Mixture of fuels approach for solution combustion synthesis of nanoscale $MgAl_2O_4$ powders, Adv. Powd. Technol. 22 (2011) 72-76.
11. A. Saberi, F. Golestani-Fard, H. Sarpoolaky, et al., Development of $MgAl_2O_4$ spinel coating on graphite surface to improve its water-wettability and oxidation resistance, Ceram. Inter. 35 (2009) 457-461.
12. [12] E. M. M. Ewais, A. A. M. El-Amir, D. H. A. Besisa, et al., Synthesis of nanocrystalline MgO/$MgAl_2O_4$ spinel powders from industrial wastes, J. All. Comp. 691 (2017) 822-833.
13. N. Obradović, W. G. Fahrenholtz, S. Filipović, et al., The effect of mechanical activation on synthesis and properties of $MgAl_2O_4$ ceramics, Ceram. Inter. 45 (9) (2019) 12015-12021.
14. P. Bar-On, I. J. Lin, S. Nadiv, et al., Formation of partially inverse Mg−Al spinel by grinding MgO with γ-Al_2O_3, J. Therm. Anal. Calorim. 42(1) (1994) 207-217.

15. J. Rufner, D. Anderson, K van Bethem, R. H. R. Castro, Synthesis and Sintering Behavior of Ultrafine (<10 nm) Magnesium Aluminate Spinel Nanoparticles, J. Am. Ceram. Soc. 96(7) (2013) 2077-2085.
16. A. Pourshamsi, A. Alhaji, R. Emadi, The effect of pre-annealing and post-annealing on the transparency of $MgAl_2O_4$, prepared by slip casting and spark plasma sintering (SPS), Ceram. Inter. 45 (2019) 7151-7156.
17. G. Kerbart, C. Harnois, C. Bilot, et al., Pressure-assisted microwave sintering: A rapid process to sinter submicron sized grained $MgAl_2O_4$ transparent ceramics, J. Eur. Ceram. Soc. 39 (2019) 2946-2951.
18. S. K. Mohan, R. Sarkar, Effect of ZrO_2 addition on $MgAl_2O_4$ spinel from commercial grade oxide reactants, Ceram. Inter. 42 (2016) 10355-10365.
19. L.-L. Zhu, Y.-J. Park, L. Gan, et al., Fabrication of transparent $MgAl_2O_4$ from commercial nanopowders by hot-pressing without sintering additive, Mater. Lett. 219 (2018) 8-11.
20. S. F. Wang, J. Zhang, D. W. Luo, et al., Transparent ceramics: Processing, materials and applications, Prog. Sol. St. Chem. 41 (2013) 20-54.
21. F. Wang, Y. Zhao, C. Yang, et al., Effect of MoO_3 on microstructure and mechanical properties of (Ti,Mo)Al/Al_2O_3 composites by in situ reactive hot pressing, Ceram. Inter. 42 (2016) 1-8.
22. C. Manière, S. Chan, G. Lee, et al., Sintering dilatometry based grain growth assessment, Res. Phys. 10 (2018) 91-93.
23. [23] W. S. Rasband, ImageJ, U. S. National Institutes of Health, Bethesda, Maryland, USA, https://imagej.nih.gov/ij/, 1997-2018.
24. I. Ganesh (2013) A review on magnesium aluminate ($MgAl_2O_4$) spinel: synthesis, processing and applications, International Materials Reviews, 58:2, 63-112, DOI: 10.1179/1743280412Y.0000000001
25. S. Pandey. V. Buljak, I. Balać, Reduced order numerical modeling for calibration of complex constitutive models in powder pressing simulations, Sci. Sinter. 49 (2017) 331-345.
26. H. G. Kin, O. Gillia, D. Bouvard, A phenomenological constitutive model for the sintering of alumina powder, Journal of the European Ceramic Society, 23(10) (2003) 1675-1685.
27. Simulia Inc, ABAQUS: Standard, Theory and User's manuals, Release 6.13, Province, RI 02909, USA, 2013.
28. N. Labus, Z. Vasiljević, O. Aleksić, et al., Characterisation of $Mn_{0.63}Zn_{0.37}Fe_2O_4$ Powders After Intensive Milling and Subsequent Thermal Treatment, Sci. Sinter. 49 (2017) 455-467.
29. N. Obradović, M. Gigov, A. Đorđević, et al., Shungite – a carbon-mineral rock material: Its sinterability and possible applications, Proc. Appl. Ceram. 13 [1] (2019) 89-97.
30. S. Filipović, N. Obradović, S. Marković, et. al., The effect of ball milling on properties of sintered manganese-doped alumina, Adv. Powd. Technol. 30 (2019) 2533-2540.
31. N. Obradović, S. Filipović, N. Đorđević, et. al., Microstructural and Electrical Properties of Cordierite-based Ceramics Obtained After Two-step Sintering Technique, Sci. Sinter. 48 (2016) 157-165.
32. J. Živojinović, V. P. Pavlović, N. J. Labus, et. al., Analysis of the Initial-Stage Sintering of Mechanically Activated $SrTiO_3$, Sci. Sinter. 51 (2019) 199-208.
33. D. A. Kosanović,V. A. Blagojević, N. J. Labus, et. al., Effect of Chemical Composition on Microstructural Properties and Sintering Kinetics of (Ba,Sr)TiO_3 Powders, Sci. Sinter., 50 (2018) 29-38.

34. N. Obradović, W. G. Fahrenholtz, S. Filipović, et. al., Formation kinetics and cation inversion in mechanically activated $MgAl_2O_4$ spinel ceramics, J. Therm. Anal. Calorim., http://link.springer.com/article/10.1007/s10973-019-08846-w
35. E. M. M. Ewais, A. A. M. El-Amir, D. H. A. Besisa, et. al., Synthesis of nanocrystalline $MgO/MgAl_2O_4$ spinel powders from industrial wastes, J. All. Comp. 691 (2017) 822-833.
36. V. Buljak, G. Bruno, Numerical modeling of thermally induced microcracking in porous ceramics: An approach using cohesive elements, Journal of the European Ceramic Society, 38 (2018) 4099-4108.

Садржај: *Јединствена кристална фаза $MgAl_2O_4$ је добијена из смеше MgO-Al_2O_3 механичком активацијом. Смеше прахова MgO и Al_2O_3 су активиране у млину у атмосфери ваздуха, током 30, 60, 90 и 120 минута. Циљ овог експеримента је била анализа фазног састава, микроструктуре и денсификације синтерованих узорака. Након синтеровања у дилатометру на 1500 °C, XRD и SEM анализе су урађене. Резултати су показали да је механичка активација ефикасан метод да се побољша денсфикација синтерованих узорака $MgAl_2O_4$, и механичка активација помера почетак синтеровања за око 100 ^oC. На основу дилатометрије, узорци су синтеровани топлим пресовањем на 1450 ^oC. Готово сви узорци су достигли 100 % теоријске вредности, док узорак активиран 30 минута има најбржу денсификацију.*

Кључне речи*: механичка активација; синтеровање; XRD; SEM; спинел.*